



## The effects of discrete conductive blocks on the natural convection in side-heated open cavities

Admilson T. Franco<sup>a,\*</sup>, Paulo R.M. Santos<sup>a</sup>, Alan Lugarini<sup>a</sup>, Leonardo T. Loyola<sup>a</sup>,  
Fernando C. De Lai<sup>a</sup>, Silvio L.M. Junqueira<sup>a</sup>, Vanessa G. Nardi<sup>b</sup>, Marcelo M. Ganzarolli<sup>c</sup>,  
José L. Lage<sup>d</sup>

<sup>a</sup> Research Center for Rheology and Non-Newtonian Fluids (CERNN) Postgraduate Program in Mechanical and Materials Engineering Federal University of Technology – Paraná (UTFPR) Curitiba, PR, 81280-340, Brazil

<sup>b</sup> Institute of Metallurgy Clausthal University of Technology Robert-Koch-Str. 42, 38678 Clausthal-Zellerfeld, Germany

<sup>c</sup> State University of Campinas Mechanical Engineering School Energy Department, Campinas-SP, 13083-970, Brazil

<sup>d</sup> Mechanical Engineering Department Lyle School of Engineering Southern Methodist University, Dallas-TX, 75275-0337, USA

### ARTICLE INFO

#### Keywords:

Natural convection  
Open cavity  
Heterogeneous model  
Nusselt correlation  
Heat Transfer

### ABSTRACT

This study considers the thermo-hydraulic effects of discrete solid blocks on the natural convection inside a fluid filled, horizontally heated side-open cavity. The cavity, having adiabatic horizontal surfaces and an isothermal hot wall, is open to a vast reservoir filled with a quiescent fluid maintained at a temperature lower than the cavity wall temperature. A fixed amount of solid material is progressively distributed inside the cavity as disconnected and conductive square blocks of different numbers and sizes, forming a uniform square lattice. The ensuing natural convection process is modeled analytically considering the fluid and solid constituents inside the cavity separately, and simulated through a validated numerical approach following a parametric analysis done in terms of the Rayleigh number ( $10^5 \leq Ra \leq 10^8$ ), the total number of blocks ( $9 \leq N \leq 144$ ) and the solid-to-fluid thermal conductivity ratio ( $0.1 \leq \kappa \leq 100$ ). The cavity aspect ratio and fluid Prandtl number are kept equal to unity, and the volume-fraction of the solid constituent is equal to 0.36. The present study evaluates the thermo-hydraulic effects of the blocks in the permanent convection process through streamlines, isotherms, hot wall Nusselt mean number and dimensionless mass flow through the fluid reservoir cavity. The blocks affect the convection process in three ways: via channeling, flow interference, and discontinuous fin-like diffusion. The most important effect is interference, which is shown to be analytically predictable. The fin-like effect is the most complex and modulates mostly by the magnitude of  $\kappa$ . Finally, analytical correlations are presented for averaged hot-wall Nusselt number and the nondimensional mass flow rate as useful practical tools in helping the design and analysis of similar configurations.

### 1. Introduction

Heat transfer by convection in cavities is a growing subject in the scientific community. It can be observed in recent years, several works with different aspects of convection, e.g., conjugated natural convection of hybrid nanofluids [1], magnetized flow in square cavities [2], laminar convection through a vertical cylinder filled with phase change materials [3], forced convection in a bifurcated channel with porous regions [4], natural convection in a semi-elliptical cavity [5]. Many authors

have been interested in investigating natural convection in cavities open on the side, commonly known to be a ubiquitous process found in a wide range of engineering applications, such as in building insulation, solar receivers, ventilation, oil and gas production wells, cooling of electronic, and materials and food processing [6].

One of the first relevant works on this subject was by Penot [7], who examined the effects of the Grashof number, among others, on free convection flow inside an isothermal open square cavity. Chan and Tien [8] studied the natural convection inside a side-open enclosure with one heated wall and adiabatic horizontal surfaces. The numerical

\* Corresponding author.

E-mail addresses: [admilson@utfpr.edu.br](mailto:admilson@utfpr.edu.br) (A.T. Franco), [paulosantos.2017@alunos.utfpr.edu](mailto:paulosantos.2017@alunos.utfpr.edu) (P.R.M. Santos), [alansouza@utfpr.edu.br](mailto:alansouza@utfpr.edu.br) (A. Lugarini), [leonardo.loyola@hotmail.com](mailto:leonardo.loyola@hotmail.com) (L.T. Loyola), [fernandodelai@utfpr.edu.br](mailto:fernandodelai@utfpr.edu.br) (F.C. De Lai), [silvio@utfpr.edu.br](mailto:silvio@utfpr.edu.br) (S.L.M. Junqueira), [vanessa.glueck.nardi@tu-clausthal.de](mailto:vanessa.glueck.nardi@tu-clausthal.de) (V.G. Nardi), [ganza@fem.unicamp.br](mailto:ganza@fem.unicamp.br) (M.M. Ganzarolli), [JLL@smu.edu](mailto:JLL@smu.edu) (J.L. Lage).

<https://doi.org/10.1016/j.applthermaleng.2022.119613>

Received 6 May 2022; Received in revised form 13 October 2022; Accepted 2 November 2022

Available online 12 November 2022

1359-4311/© 2022 Elsevier Ltd. All rights reserved.

Nomenclature	
$a, b, c$	curve fitting coefficients
$A$	cavity aspect ratio
$D$	nondimensional block side length
$g$	gravitational acceleration, [ $m/s^2$ ]
$h_{av}$	average heat transfer coefficient, [ $W/m^2K$ ]
$H$	enclosure height, [ $m$ ]
$\mathbf{i}, \mathbf{j}$	unit vectors in the $x$ - and $y$ -directions
$k$	thermal conductivity, [ $W/mK$ ]
$L$	enclosure length, [ $m$ ]
$\dot{m}_{in}$	nondimensional mass flow rate into the cavity
$\mathbf{n}$	surface normal unit vector
$N$	number of solid blocks
$Nu_{av}$	average hot wall Nusselt number
$p$	pressure, [ $Pa$ ]
$P$	non-dimensional pressure
$Pr$	Prandtl number
$Ra$	Rayleigh number
$S_B$	nondimensional distance from cavity surfaces to the nearest solid block
$S^*$	nondimensional boundary layer thickness
$T$	temperature, [ $K$ ]
$T_o$	fluid reservoir temperature, [ $K$ ]
$T_H$	cavity wall temperature, [ $K$ ]
$u, v$	$x$ and $y$ Cartesian velocity components, [ $m/s$ ]
$\mathbf{v}$	velocity vector
$U, V$	nondimensional Cartesian velocities components
$\mathbf{V}$	nondimensional velocity vector
$x, y$	horizontal and vertical Cartesian coordinates, [ $m$ ]
$X, Y$	non-dimensional Cartesian coordinates
<i>Greek symbols</i>	
$\alpha$	thermal diffusivity, [ $m^2/s$ ]
$\beta$	isobaric coefficient of volumetric thermal expansion, [ $1/K$ ]
$\phi$	fluid volume fraction
$\kappa$	solid-to-fluid thermal conductivity ratio
$\mu$	fluid dynamic viscosity, [ $kg/ms$ ]
$\nu$	fluid kinematic viscosity, [ $m^2/s$ ]
$\theta$	non-dimensional temperature
$\rho$	density, [ $kg/m^3$ ]
$\omega$	volume [ $m^3$ ]
$\Psi$	non-dimensional streamfunction
<i>Subscripts</i>	
$f$	fluid
$H$	hot
$in$	entering the domain
$min$	minimum
$max$	maximum
$out$	leaving the domain
$s$	solid or block
$T$	total

simulations were performed using a domain extended well into the fluid reservoir region outside the cavity. Chan and Tien [9] extended their prior study to a rectangular shallow open cavity with an aspect ratio  $A = 7$ , with the numerical results for  $Ra = 103$ – $106$  agreeing well with experimental data. Angirasa et al. [10] reported a detailed numerical calculation for an isothermal cavity open on one side using a truncated domain that excluded the region outside the cavity. Bilgen and Muf-tuoglu [11] investigated the heat transfer process in an open square cavity in which the wall was subjected to uniform heat flux, and the two horizontal surfaces were insulated. The cavity is connected to an external fluid reservoir via multiple ventilation slots. An optimum opening ratio at high Rayleigh numbers was found for a given number of slots. Investigations on combined mixed natural convection and radiation heat transfer in open cavities have been addressed as well [12–14], with radiation being found to play an important role when the absolute temperature difference within the cavity is large ( $\Delta T \geq 200$  K).

More recently, interest in the presence of solid obstacles within an open cavity has intensified. Chacon et al. [15] studied a heated solid block positioned into an open cavity, focusing on vortex formation mechanisms. Vortical separation from the boundary layer over the block, shedding from thermal plumes, and recirculating in cavity corners were observed. Lugarini et al. [16] investigated the combination of natural convection and surface radiation processes in a similar configuration, considering a single square block in a side-open cavity. Numerical results showed the block size to significantly impact the amount of radiation exchanged between the cavity's heated wall and the exterior, allowing the modulation of the total heat transfer via the selection of an appropriate block sizing. Note that the study of natural convection in side-open cavities with a single solid inside the cavity is an evolution of the fully enclosed (no opening) configuration with a single block of fixed [17–20] and variable aspect ratios [21–24].

Enclosed cavities with different amounts of blocks are even more interesting and practical problems, being studied with the percolation of Newtonian fluids [25–28], nanofluids [29] and viscoplastic fluids [30]. As discussed later, the present project is the analytical expression

predicting the interference limit of the solid obstacles on the natural convection inside the enclosure proposed by Merrikh and Lage [31]. This configuration is akin to fractures found in oil and gas reservoir drilling and production, which can also be tackled following a porous medium approach [32,33].

The present project extends the geometric configuration to consider a side-open cavity now filled not only by fluid but also with disconnected and participating (from a heat transfer point-of-view) discrete solid blocks. As the number of solid blocks inside the cavity is relatively small, a continuum approach (as opposed to a porous-continuum approach [34]) is retained for modeling the natural convection process inside the open-side cavity, with the two constituents – fluid and solid – considered separately. Notice the continuum approach also benefits from yielding detailed insights into the solid–fluid interactions, which can be significant for enhanced oil recovery applications, for instance.

## 2. Problem description and mathematical model

The square-shaped, side-open cavity considered here is shown schematically in Fig. 1. The left wall of the cavity, with height  $H$ , is assumed isothermal, maintained at a constant and uniform temperature,  $T_H$ , with the fluid in the large surrounding reservoir far from the cavity (accessed through the right opening of the cavity, distant  $L$  units from the left wall) maintained at  $T_o$ . The surrounding fluid surrounding fluid fills the cavity fills the cavity, and it contains several conducting, disconnected and uniformly distributed square blocks forming a square lattice. Observe that the perpendicular distance between two consecutive blocks is twice the distance between a cavity surface and an adjacent block. Also, because the natural convection process inside the cavity entails draining fluid from, and discharging fluid into the surrounding reservoir, the computational domain for performing numerical simulations is extended beyond the cavity, as shown in Fig. 1, with a total length  $2L$  and a total height  $3H$ .

This choice of an extended domain has been determined via numerical tests to yield a good compromise between computational time

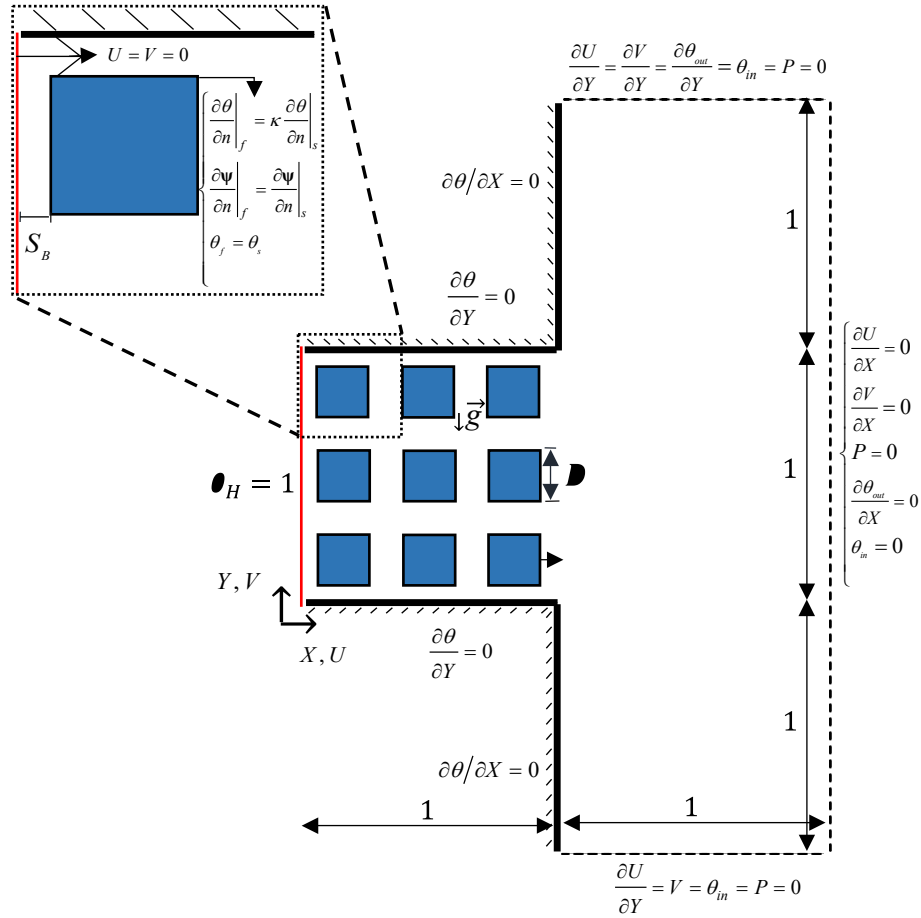


Fig. 1. Schematic representation of the side-open cavity with extended domain and boundary conditions.

and independence of the results concerning the imposed boundary conditions in the outside reservoir [3].

With the side-open cavity considered square (aspect ratio  $A = L/H = 1$ , as shown in Fig. 1 the transport balance equations modeling the natural convection process, for each one of the two constituents (fluid and solid), assuming incompressible Newtonian fluid with constant and homogeneous properties, Boussinesq-Oberbeck approximation for the buoyancy effect, steady-state, are [35]:

$$\nabla \cdot \mathbf{v} = 0 \quad (1)$$

$$\rho_f (\mathbf{v} \cdot \nabla) \mathbf{v} = -\nabla p + \mu \nabla^2 \mathbf{v} + \rho_f g \beta (T - T_0) \mathbf{j} \quad (2)$$

$$(\rho c)_f (\mathbf{v} \cdot \nabla T) = k_f \nabla^2 T \quad (3)$$

$$0 = k_s \nabla^2 T \quad (4)$$

Equation (1) is the continuity equation, while Eqs. (2) and (3) are the momentum and energy balance equations for the fluid. Equation (4) is the energy balance equation for the solid blocks. The system of Eqs. (1)-(4) can be nondimensionalized using coordinates  $(X, Y) = (x, y)/H$ , fluid velocity  $\mathbf{V}$  with components,  $(U, V) = (u, v)/(\alpha_f/H)$ , pressure  $P = p H^2 / \rho_f (\alpha_f)^2$ , and temperature  $\theta = (T - T_0)/(T_H - T_0)$ . The resulting equations are [8]:

$$\nabla \cdot \mathbf{V} = 0 \quad (5)$$

$$(\mathbf{V} \cdot \nabla) \mathbf{V} = -\nabla P + Pr \nabla^2 \mathbf{V} + Ra Pr \theta \mathbf{j} \quad (6)$$

$$(\mathbf{V} \cdot \nabla \theta) = \nabla^2 \theta \quad (7)$$

$$\nabla^2 \theta = 0 \quad (8)$$

where Eqs. (5)-(7) apply at the fluid region, eq. (8) at the solid blocks, and the additional parameters are the Prandtl number,  $Pr = \nu/\alpha_f$ , and the Rayleigh number,  $Ra = g\beta H^3(T_H - T_0)/(\nu \alpha_f)$ , with  $\alpha_f$  and  $\nu$  being thermal diffusivity and kinematic viscosity of the fluid, respectively. The corresponding non-dimensional boundary conditions and the boundary conditions for the solid blocks are shown in Fig. 1. Keep in mind the boundary conditions for the blocks, i.e., non-slip, impermeable, and continuous temperature and heat flux, are in fact “internal” compatibility conditions imposed at the solid–fluid interfaces [26], respectively:

$$U = V = 0, \theta_f = \theta_s, \frac{\partial \theta}{\partial \mathbf{n}_f} = \kappa \frac{\partial \theta}{\partial \mathbf{n}_s} \quad (9)$$

where  $\mathbf{n}$  is the unit vector normal to each block surface, and  $\kappa = k_s/k_f$  is the solid-to-fluid thermal conductivity ratio. Notice that the chosen nondimensionalization yields balance Eqs. (7) and (8) independent of the parameter  $\kappa$ , which shows up only in the heat-flux compatibility condition listed in eq. (9).

The convection strength inside the cavity is monitored using the wall-averaged Nusselt number, defined as [36]:

$$Nu_{av} = \frac{h_{av} H}{k_f} = \int_{X=0}^1 \left( -\frac{\partial \theta}{\partial X} \right) dY \quad (10)$$

where  $h_{av}$  is the average heat transfer coefficient obtained by energy conservation in a surface adjacent to the wall. It can be obtained by integrating the local heat transfer coefficient  $h(x)$  along the heated wall:

**Table 1**  
Summary of parameter values.

$Ra$	$10^5, 10^6, 10^7, 10^8$
$k$	0.1, 1, 10, 100
$(N,D)$	(9,0.2), (16,0.15), (36,0.1), (64,0.075), (144,0.05)

$$\bar{h} = 1/H \int_0^H h(y)dy \quad (11)$$

The nondimensional mass flow rate,  $\dot{m}_{in}$ , entering the cavity through the side opening [3]:

$$\dot{m}_{in} = - \int_{X=1} U dY \quad (12)$$

where  $U = 0$  if  $U \geq 0$  (mass leaving the cavity).

Finally, the dimensionless stream function is calculated as:

$$\Psi(X, Y) = - \int_{X_o}^X V(X, Y) dX + \Psi(X_o, Y_o) \quad (13)$$

with the reference value  $\Psi(X_o, Y_o)$  set as zero along the solid surfaces of the cavity.

### 3. Results and discussion

The balance equations (5)-(8), with the described boundary and compatibility conditions, were solved using a second-order finite volume method, with a hybrid scheme for the discretization of the advective terms and the SIMPLEST algorithm for the pressure-velocity coupling (Patankar[37] and Versteeg and Malalasekera[38]). A residual control criterion establishes convergence whenever the sum of all absolute residues of each variable ( $U, V, P$ , and  $\theta$ ) is less than  $10^{-6}$ .

The aspect ratio of the cavity and the fluid Prandtl number are set to  $A = Pr = 1$ , the number  $N$  of blocks (forming a square lattice inside the cavity) varies from 9 to 144, the Rayleigh number,  $Ra$ , from  $10^5$  to  $10^8$ , and the solid-fluid thermal conductivity ratio  $\kappa$  from 0.1 to 100. The effect of the solid blocks is examined for a fixed fluid-fraction (or porosity) of the cavity,  $\phi = \omega_f / \omega_T = 0.64$ , where  $\omega_f$  and  $\omega_T$  are the fluid and the total volume inside the cavity, respectively. By fixing the fluid-fraction (and by consequence the solid-fraction, equal to  $(1-\phi)$ ), the size of the square blocks (nondimensional side length  $D$ ) becomes directly linked to the number of blocks  $N$  via  $D = [(1-\phi)/N]^{0.5}$  [26]. Another interesting aspect of this choice of block parameters becomes evident when the number of blocks increases inside the cavity: to maintain the same solid-fraction, the block size has to decrease. This is akin to having the fixed amount of solid constituent being distributed inside the cavity in a progressively finer (more and smaller blocks) manner. Table 1 summarizes the parametric space set for the numerical simulations, including the pairs  $(N,D)$ .

The modeling and numerical simulation procedures are validated via comparison with existing published results, considering first the case of a fluid saturated enclosure containing discrete solid blocks [31,39], and second the case of an open cavity filled with a clear (of blocks) fluid [8,40]. Results for the first case comparison are shown in Table 2, and

**Table 2**  
Average  $Nu_{av}$  for enclosure with  $N$  blocks, various  $Ra$ , with  $A = Pr = \kappa = 1$ .

$N$	$Ra = 10^5$			$Ra = 10^6$			$Ra = 10^7$			$Ra = 10^8$		
	[31]	[39]	present	[31]	[39]	present	[31]	[39]	present	[31]	[39]	present
9	1.383	1.405	1.389	6.164	6.277	6.232	16.087	15.931	16.001	31.797	30.545	31.105
16	1.233	1.251	1.241	4.274	4.385	4.341	15.258	15.142	15.234	31.180	30.132	30.780
36	1.098	1.113	1.104	2.626	2.682	2.635	11.789	11.928	11.984	30.689	29.600	30.327
64	1.051	1.053	1.046	2.223	2.249	2.190	8.094	8.096	8.040	29.394	28.137	28.659
144	1.013	—	1.013	1.632	—	1.651	5.181	—	5.317	20.040	—	20.991

**Table 3**  
Average  $Nu$  and inlet flow rate for the open cavity, various  $Ra$ , with  $A = Pr = 1$ .

$Ra$	$Nu_{av}$			$\dot{m}_{in}$	
	[8]	[40]	present	[8]	present
$10^3$	1.07	—	1.051	1.95	1.914
$10^4$	3.41	3.57	3.406	8.02	7.953
$10^5$	7.69	7.75	7.701	21.1	20.997
$10^6$	15.0	15.11	15.003	47.3	45.550
$10^7$	28.6	28.70	27.932	96.0	90.046
$10^8$	56.8	—	51.270	190	172.055

Table 3 shows results for the second case, both with excellent agreement.

Based on a mesh test, a maximum permissible relative error between two consecutive levels of mesh of less than 1.5 % was adopted for both  $Nu_{av}$  and  $\dot{m}_{in}$ . To generate a suitable mesh that would respect the mesh

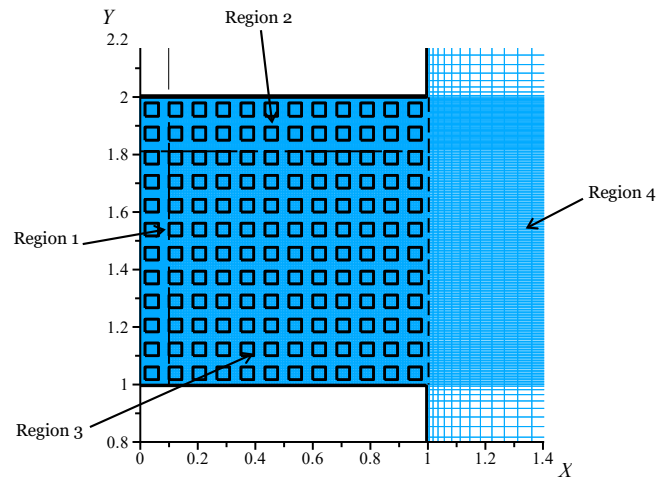


**Fig. 2.** Mesh distribution in the square open cavity and around the opening illustrating the different regions of mesh refinement and the high concentration of points near the hot wall and upper wall for  $Ra = 10^8$  and  $N = 144$ .

**Table 4**  
Mesh independence test for region 3.

Parameter studied	Meshes $M$ and percentage errors $EP$				
	$M = 60$	$EP$	$M = 120$	$EP$	$M = 180$
$Nu_{av}$	38.3977	0.8854 %	38.0607	0.6677 %	37.8083
$\dot{m}_{in}$	94.8685	3.3374 %	91.8046	1.4586 %	90.4848

**Table 5**  
Mesh independence test for region 1.

Parameter studied	Meshes $M$ and percentage errors $EP$				
	$M = 300$	$EP$	$M = 360$	$EP$	$M = 480$
$Nu_{av}$	37.1591	1.5664 %	36.586	0.7299 %	36.7180
$\dot{m}_{in}$	90.4848	0.4437 %	90.8880	0.2901 %	90.6252

**Table 6**  
Mesh independence test for region 2.

Parameter studied	Meshes $M$ and percentage errors $EP$				
	$M = 180$	$EP$	$M = 240$	$EP$	$M = 360$
$Nu_{av}$	36.586	0.3094 %	36.4731	0.1308 %	36.4255
$\bar{min}$ ,	90.888	2.0037 %	89.1026	0.6391 %	88.5368

independence criteria while at the same time avoiding prohibitive simulation times, the sensitivity of the solution to mesh refinement in the following four different regions of the numerical domain was tested: 1 - the region near the heated wall; 2 - the region near the upper adiabatic wall; 3 - the region corresponding to the remainder of the cavity; and 4 - the region outside the cavity. This division of the numerical domain is illustrated in Fig. 2 for a mesh using  $Ra = 10^8$  and  $N = 144$ . It is important to stress that each control volume contains only one phase:

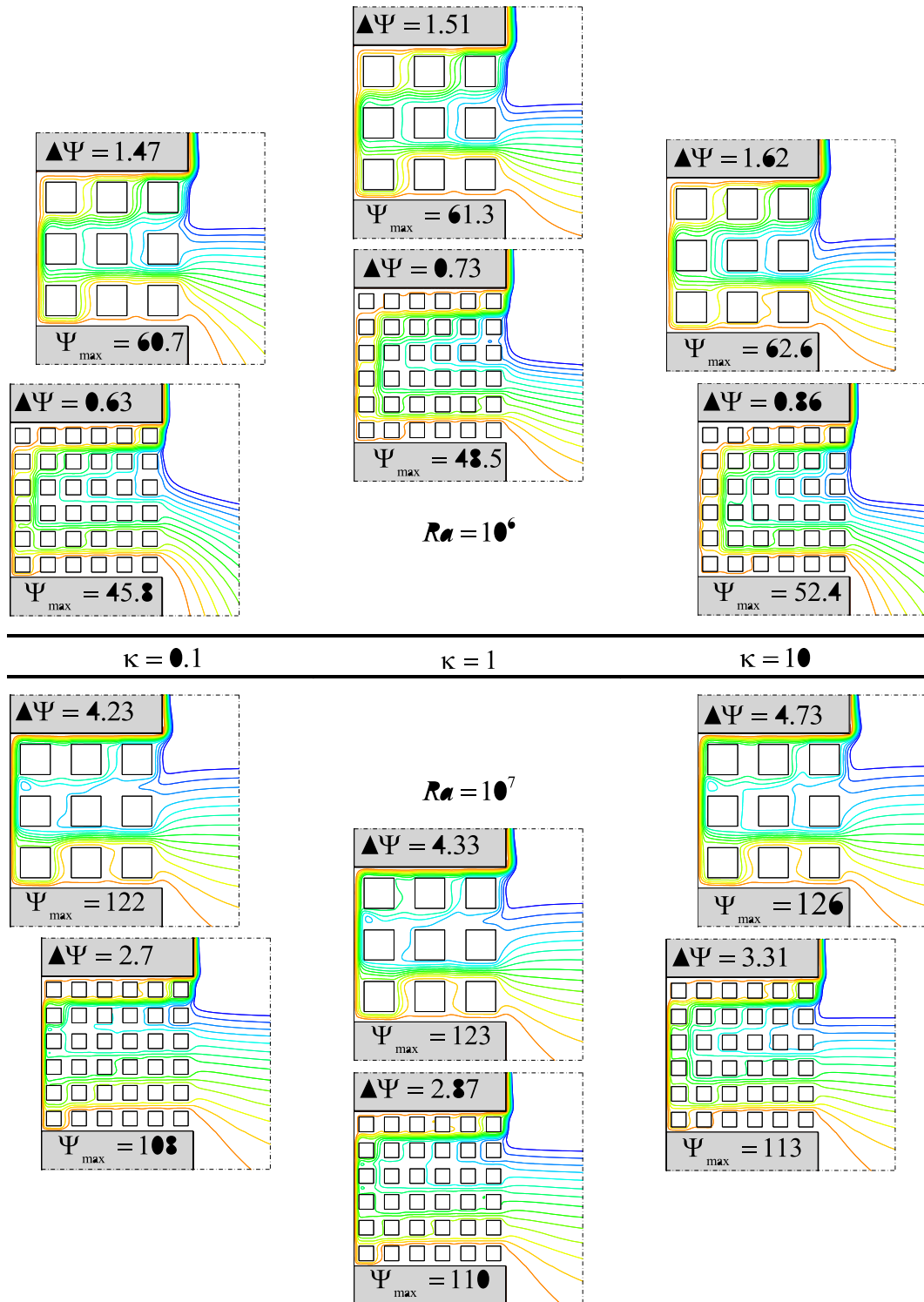


Fig. 3. Sample streamlines for  $Ra = 10^6, 10^7, N = 9, 36, \kappa = 0.1, 1, \text{ and } 10$ .

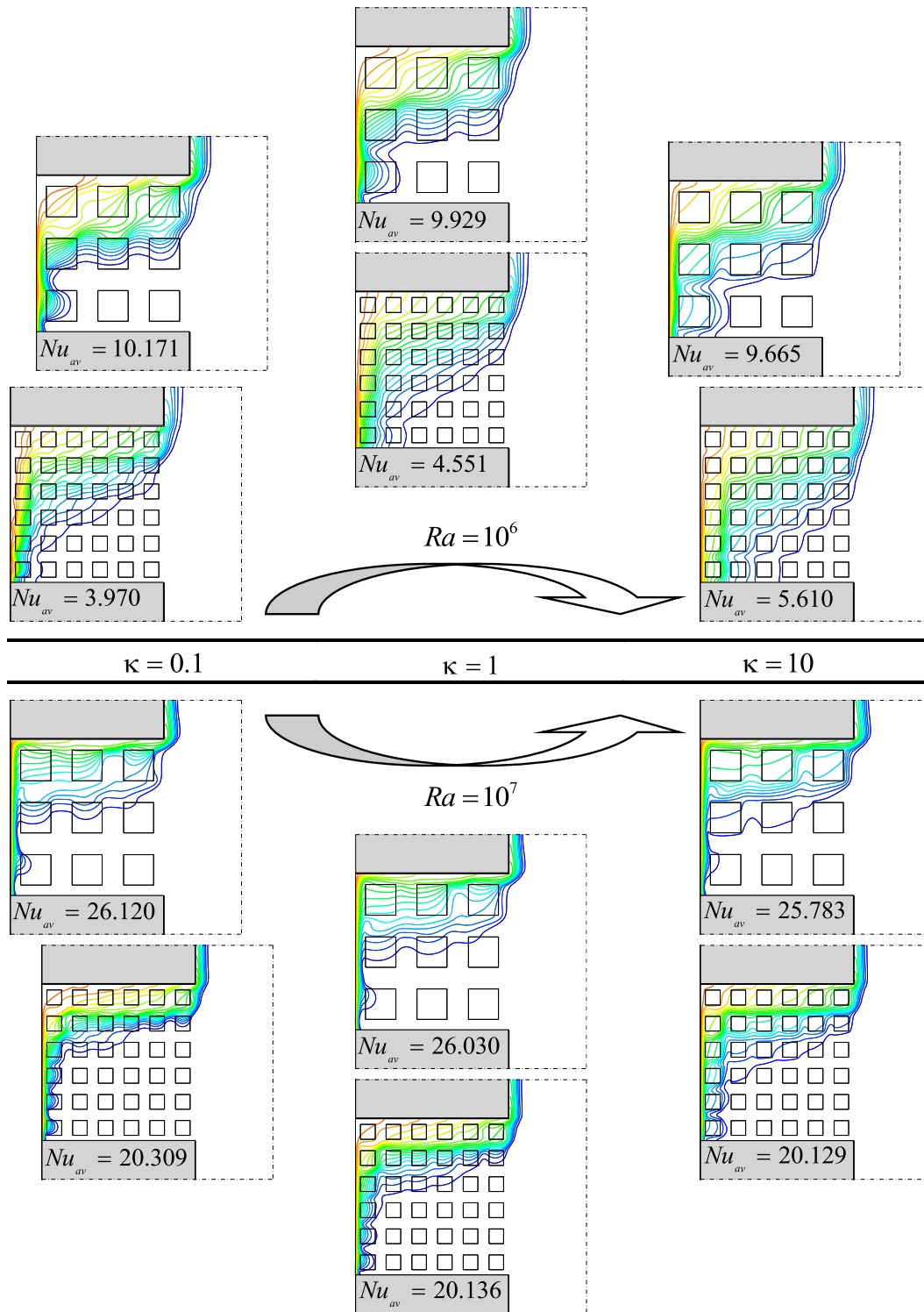


Fig. 4. Sample isotherms for  $Ra = 10^6, 10^7, N = 9, 36, \kappa = 0.1, 1, \text{ and } 10. \theta$  range from 0 to 0.95, with  $\Delta\theta = 0.05$ .

either a solid or a fluid one.

Table 4 shows the mesh test performed for region 3, the base mesh for the entire cavity, from which the meshes of the other regions are refined. Due to the high value of the error for  $\dot{m}_{in}$ , exceptionally in this case the finer mesh was adopted,  $M = 180$ . After determined the mesh for region 3, we started to define the mesh in region 1. Table 5 presents the results found. The appropriate mesh is  $M = 360$  for region 1. Continuing the mesh test, the refining study was performed for region 2. Table 6 presents the results found, adopting the mesh  $M = 240$  for region

2.

Although the modeling presented in the balance eqs (5)-(9) is valid for a steady-state, some additional tests were performed for some of the most stringent cases, e.g.,  $Ra = 10^8, \kappa = 100$  and  $N = 9$ , using an unsteady model. The results show  $Nu_{av}$  to be within 0.3 % of the steady-state results, validating the steady assumption of the original model for the entire parametric range used here.

Fig. 3 shows streamlines for  $Ra = 10^6$  and  $10^7, N = 9$  and  $36, \text{ and } \kappa = 0.1, 1$  and  $10$ . The first observation is very subtle: the effect of changing

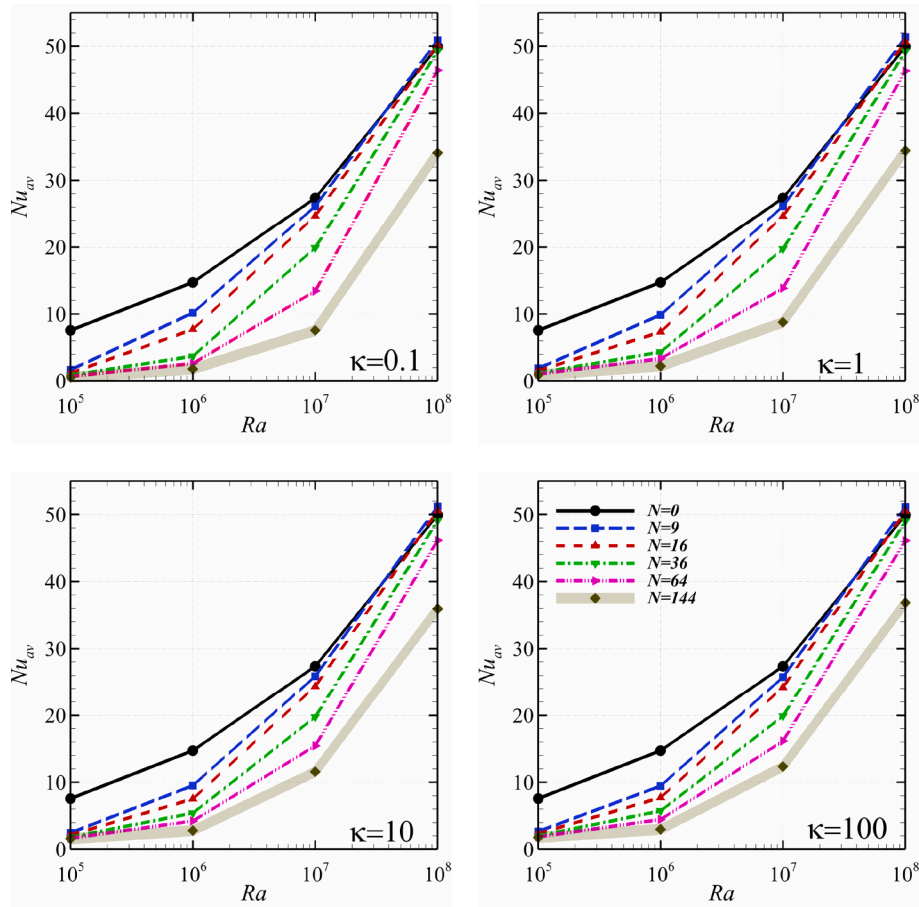


Fig. 5.  $Nu_{av}$  versus  $Ra$  number for various  $N$  and  $\kappa$ .

$\kappa$  seems minor, increasing the convection intensity slightly inside the cavity when  $\kappa$  varies from 0.1 to 10 – observe how the rightmost streamlines move a little lower concerning the blocks. As  $\kappa$  increases, the solid blocks change from hindering the heat diffusing from the left wall to helping it, spreading the buoyancy driving force across the cavity. Fig. 4, showing the corresponding isotherms, confirms this observation: observe how the isotherms spread from the hot wall toward the cavity opening as  $\kappa$  increases becoming more vertical (stronger diffusion).

Another observation with respect to Figs. 3 and 4 have to do with the number and size of the blocks: when  $N = 9$ , the flow is induced towards the bottom of the cavity by the heated wall and enters mainly through the lower horizontal channel formed by the first two rows of solid blocks. When it touches the heated wall, the fluid stream combines with the fluid coming up from the bottom of the heated wall and is carried upwards. The flow rises beside the heated wall, and the most part, turns right before reaching the upper horizontal wall, when it flows through the last horizontal channel of blocks and leaves the cavity to rise alongside the external vertical wall. The main stream divides when it reaches the upper right block and combines again as it leaves the cavity in the top right corner. Before it even enters the cavity, part of the fluid drawn towards the cavity is carried away by the stream that has just left it. When the number of blocks is increased to  $N = 36$ , the stream entering the cavity tends to be concentrated mainly between the horizontal channels formed by the first and second rows and the second and third rows of blocks. The fluid barely touches the heated wall, which goes up through the pathway formed between the columns of blocks nearest the heated wall. To leave the cavity, the fluid takes the path formed by the two upper rows of blocks, rising next to the external vertical wall and forming a plume thinner than that for  $N = 9$ . When  $N = 36$  the streamlines indicate that the fluid hardly reaches the vertical

wall. This is because of the restriction imposed by the shorter distance between the vertical wall and the first column of blocks compared with the distance between any two blocks.

The isotherms of Fig. 4 respond accordingly, being more vertical (parallel) to the hot wall signaling weaker convective. The isotherms waviness at the channels between the blocks, when  $N = 9$ , shows the strong channeling effect caused by the blocks.

Finally, the effect of increasing  $Ra$ , as expected, is to strengthen the convection effect as seen by the agglomeration of streamlines along the hot wall. Notice the inlet and outlet flows from/to the fluid reservoir predominate along the channels away from the horizontal surfaces of the cavity, where less resistance is found. This aspect seems independent of  $N$  and  $\kappa$ .

Fig. 5 presents  $Nu_{av}$  versus  $Ra$  for various  $N$  and  $\kappa$ . Notice results for the clear (of blocks) cavity,  $N = 0$ , are also included for completeness. Visible in Fig. 5 is the effect of the blocks tends to become negligible as  $Ra$  increases from  $10^7$  and  $10^8$  and  $N$  varies from 36 to 9. On the other hand, when  $Ra = 10^5$ , the results for the high number of blocks, i.e.,  $N = 64$  and  $144$ , indicate a conduction-dominated regime as  $Nu_{av}$  is near unity and  $\min$ , becomes very small (notice pure conduction with  $N = 0$  would lead to  $Nu_{av} = 1$  if the right open side of the cavity were maintained at  $T_0$ ). It can then be concluded that the heat transfer intensity is strongly affected by the number of blocks in the cavity. This behavior can be attributed to the presence of many blocks in the cavity, especially near the opening, obstructs the flow entering the cavity, reducing both fluid circulation and heat transfer.

Fig. 6 shows the corresponding nondimensional mass flow rate,  $\dot{m}_{in}$ , of the fluid entering the cavity. The results of both, Figs. 5 and 6, confirm, for a given  $N$  and  $\kappa$ , an increase in  $Ra$  always yields higher  $Nu_{av}$ , and  $\dot{m}_{in}$ . Also, increasing  $\kappa$  tends to push all curves closer to the limit  $N$

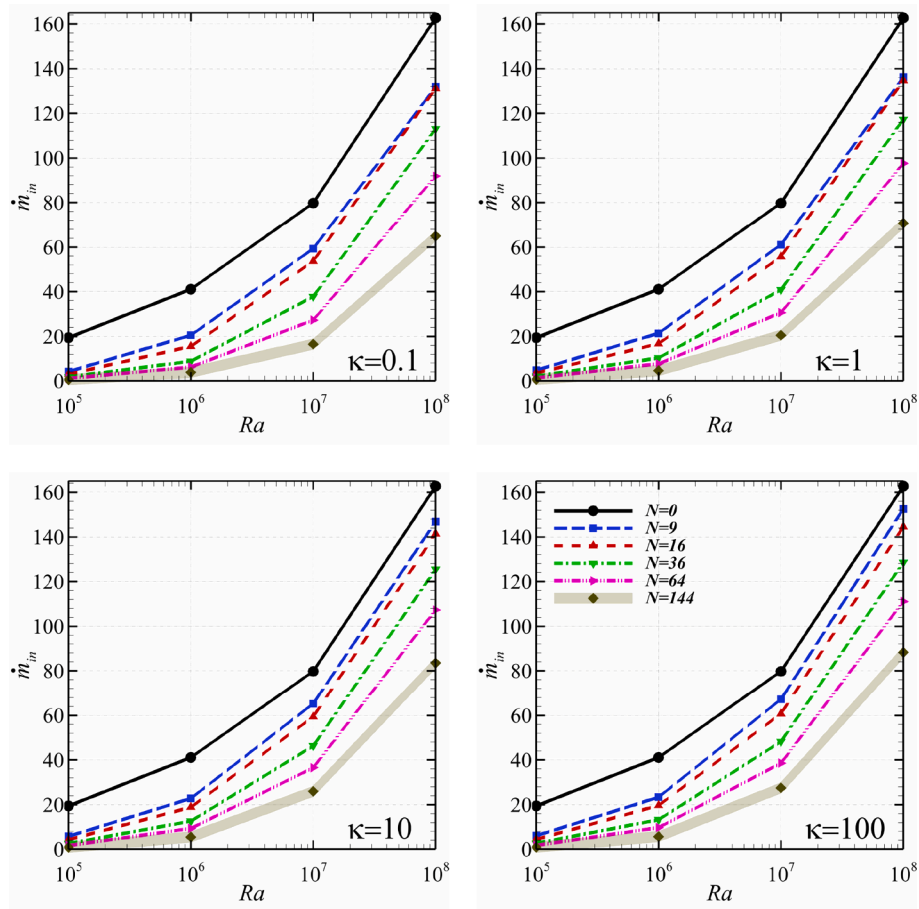


Fig. 6. Mass flow rate versus Ra number for various  $N$  and  $\kappa$ .

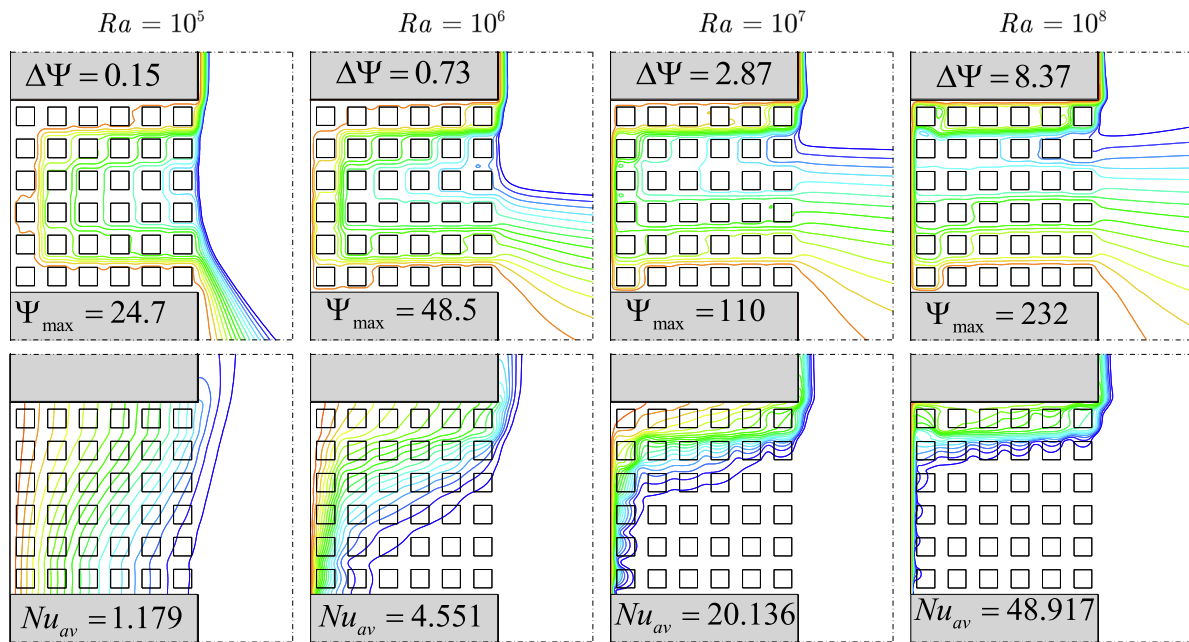


Fig. 7. Effect of  $Ra$  on  $Nu_{av}$  and the mass flow rate for  $\kappa = 1$  and  $N = 36$ . Streamlines (top) and isotherms (bottom).  $\theta$  range from 0 to 0.95, with  $\Delta\theta = 0.05$ .

$= 0$ , and a  $\kappa$  variation from 10 to 100 seems to have very minor effect on the results. In addition, increasing  $N$  increases the obstructing effect of the blocks, particularly to the inlet flow coming from the fluid reservoir,

therefore reducing both the heat transfer (Fig. 5) and the fluid circulation (Fig. 6).

The  $Nu_{av}$  values for  $N = 0$  agree well with the expression for natural

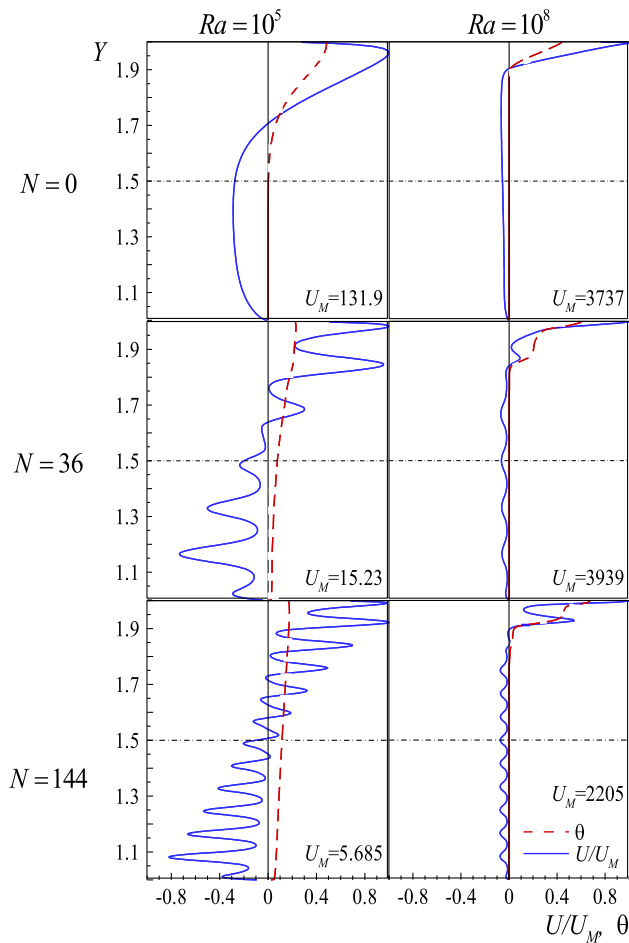


Fig. 8. Profiles of  $U$  and  $\theta$ , at the cavity opening for  $\kappa = 1$ .

convection along an isothermal vertical plate ( $Nu_{av} \sim Ra^{1/4}$ ) [36]. Thus, for the highest Rayleigh number,  $Ra = 10^8$ , the  $Nu_{av}$  can be estimated using this expression, except for  $N = 144$ . In a broad sense, one can observe three distinct ranges in Fig. 5: (1)  $N \leq 36$ , conduction seems

dominant if  $Ra \leq 10^6$ ; (2) for  $10^6 < Ra < 10^7$ : convection is dominant when  $N$  less than 64; and, (3) for  $Ra \geq 10^7$ ,  $Nu_{av}$  can be estimated reasonably from  $Nu_{av} \sim Ra^{1/4}$ .

Observe in Fig. 6 the mass flow rate,  $\dot{m}$ , seems more sensitive to variations in  $N$  and  $Ra$  than to variations in  $\kappa$ . For low  $N$  and high  $Ra$ , the results obtained for  $Nu_{av}$  and  $\dot{m}$  approach those obtained for the open cavity without blocks [8].

Fig. 7 illustrates the effect of  $Ra$  on the flow pattern,  $Nu_{av}$  and  $\dot{m}$  for  $\kappa = 1$ . When  $Ra = 10^5$  conduction is dominant, as the isotherms are only slightly distorted and the flow field appears to be symmetrical about a plane halfway up the cavity. The thermal boundary layer is thick for  $Ra = 10^6$  and thinner when  $Ra = 10^7$ , that is, it becomes thinner as  $Ra$  is increased. The boundary layer regime becomes dominant when  $Ra \geq 10^7$ , and the characteristic horizontal stratification of the isotherms can be observed. The increase in  $Ra$  produces a dramatic increase in  $\dot{m}$  (see Table 9), and the streamlines become closer to the horizontal, indicating that the stream encounters less resistance as it enters the opening. It is interesting to note that when  $Ra$  is increased from  $10^5$  to  $10^6$ , there is an approximately fourfold increase in  $Nu_{av}$ , and an approximately fivefold increase in  $\dot{m}$ . However, when  $Ra$  is increased from  $10^6$  to  $10^7$ , both  $Nu_{av}$  and  $\dot{m}$  increase by a factor of four (see Table 9 for more details). Fig. 7 also shows the complex flow pattern near the heated wall for  $Ra = 10^7$  and  $Ra = 10^8$  and near the left top corner for  $Ra = 10^8$ .

Fig. 8 shows the local variation of dimensionless horizontal fluid speed  $U$  (normalized in relation to the maximum horizontal velocity along the opening) and temperature  $\theta$  across the cavity opening for  $N = 0, 36$  and  $144$ ,  $Ra = 10^5$  and  $10^8$ , and  $\kappa = 1$ . When  $N$  increases the channeling effect caused by the blocks becomes evident by the waviness in the  $U$  profiles. As  $Ra$  increases from  $10^5$  to  $10^8$ , the flow leaving the cavity tends to concentrate near to the top surface of the cavity. The temperature profiles seem less affected by the channeling effect.

Table 7

Values of  $N_{min}$  expected for the various Rayleigh numbers.

$Ra$	$N_{min}$
$10^5$	3
$10^6$	10
$10^7$	32
$10^8$	100

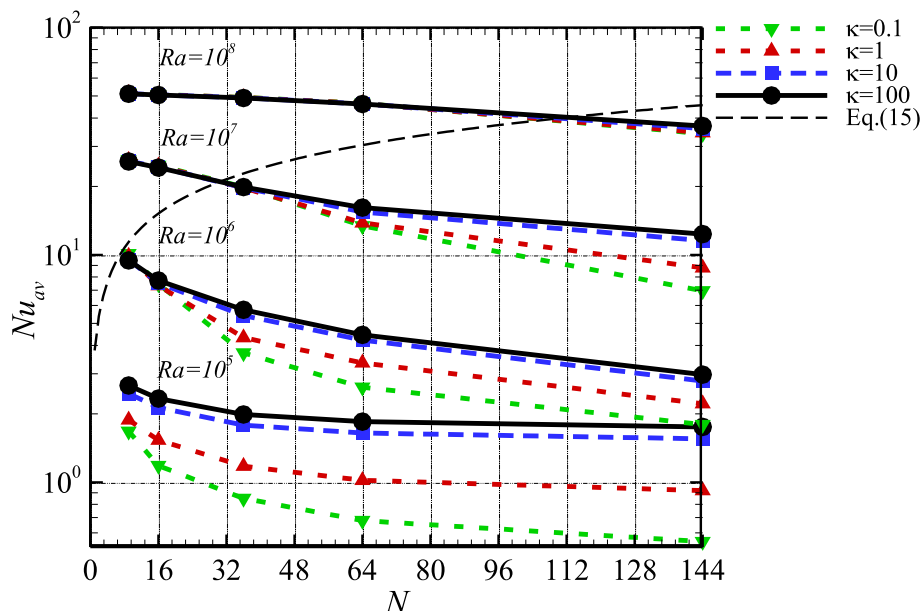


Fig. 9.  $Nu_{av}$  for various  $N$ ,  $\kappa$  and  $Ra$ .

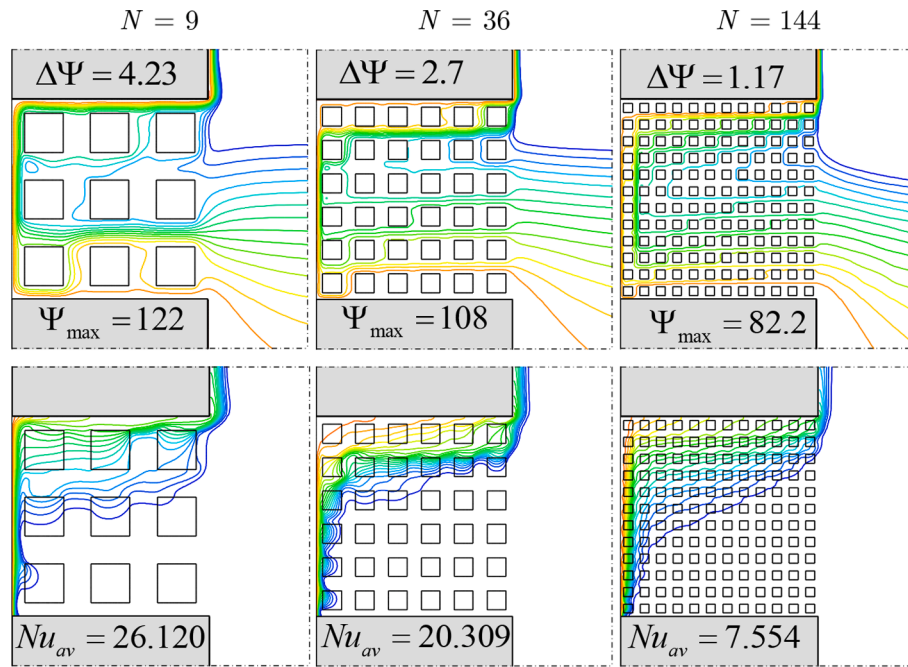


Fig. 10. Effect of the number of blocks for  $Ra = 10^7$  and  $\kappa = 0.1$ . Streamlines (top) and isotherms (bottom).  $\theta$  range from 0 to 0.95, with  $\Delta\theta = 0.05$ .

**Table 8**  
Least-square fitting parameters for eq. (16).

$Nu_{av}$			
$N$	$a$	$b$	$c$
9	$9.60 \times 10^{-2}$	$-1.19 \times 10^{-3}$	$3.41 \times 10^{-1}$
16	$5.87 \times 10^{-2}$	$-9.17 \times 10^{-4}$	$3.67 \times 10^{-1}$
36	$1.86 \times 10^{-2}$	$5.63 \times 10^{-5}$	$4.28 \times 10^{-1}$
64	$4.62 \times 10^{-3}$	$2.26 \times 10^{-3}$	$5.00 \times 10^{-1}$
144	$1.86 \times 10^{-3}$	$1.82 \times 10^{-2}$	$5.34 \times 10^{-1}$
$\dot{m}_{in}$			
$N$	$a$	$b$	$c$
9	$1.04 \times 10^{-1}$	$1.94 \times 10^{-2}$	$3.92 \times 10^{-1}$
16	$6.42 \times 10^{-2}$	$1.71 \times 10^{-2}$	$4.16 \times 10^{-1}$
36	$1.89 \times 10^{-2}$	$2.01 \times 10^{-2}$	$4.76 \times 10^{-1}$
64	$8.64 \times 10^{-3}$	$2.95 \times 10^{-2}$	$5.08 \times 10^{-1}$
144	$3.11 \times 10^{-3}$	$4.66 \times 10^{-2}$	$5.48 \times 10^{-1}$

$U_M$  represents the maximum velocity component in the  $X$ -direction at position  $X = 1$ .

Fig. 9 shows the average Nusselt number as a function of  $N$ ,  $\kappa$  and  $Ra$ . As  $N$  increases, the smaller blocks are positioned closer and closer to the hot wall. Eventually, they might get close enough to interfere with the boundary layer growing along the wall, affecting (hindering) the convection process. Hence there must be a minimum number of blocks,  $N_{min}$ , above which the blocks start to interfere with the boundary layer flow along the hot wall of the cavity.

An expression to predict the interference that the blocks promote in the thermal boundary layer can be obtained [31] by comparing the boundary layer's estimated scale along a heated (or cooled) channel wall with the space between the wall and the first column of blocks in the enclosure.

For fluids with  $Pr \geq 1$ , the boundary layer is confined to the space between two isothermal walls when  $Ra^{-1/4} \sim S^*$ , with  $S^*$  representing the dimensionless distance between the two walls. For a single isothermal wall,  $Ra^{-1/4} \sim S^*/2$  is a more appropriate scale. The dimensionless distance between the isothermal wall and the first column of blocks is:

$$S_b = \left[ 1 - (1 - \phi)^{1/2} \right] / (2N^{1/2}) \quad (14)$$

The blocks are expected to interfere with the boundary layer when  $S_B < S^*$  or when  $N > [1 - (1 - \phi)^{1/2}]^2 / (16) Ra^{1/2}$ . For  $\phi = 0.64$ , adopted in the present study, interference will occur if:

$$N_{min} \geq 0.01 Ra^{1/2} \quad (15)$$

Table 7 shows the  $N_{min}$  from eq. (15) for various  $Ra$ , and the dashed line in Fig. 9 shows eq. (15). Observe how  $Nu_{av}$  values drop precipitously as  $N$  grows beyond  $N_{min}$ , particularly for high  $Ra$ , indicating the corresponding hindrance effect of the blocks and validating the theoretical prediction, eq. (15).

Fig. 10 shows streamlines and isotherms for the case  $Ra = 10^7$ ,  $\kappa = 1$ , as  $N$  increases from 9 to 36 to 144. Notice from Table 7,  $N_{min}$  in this case is predicted to equal 32. Indeed, the compressing of the isotherms along the hot wall, indicating strong convection, is clearly seen to peak around for  $N = 36$ .

In Appendix A the numerical results of  $Nu_{av}$  and  $\dot{m}_{in}$  for  $Ra$ ,  $N$ , and  $\kappa$  have been tabulated for archival purposes. To aid thermal engineers in the design of related systems, a functional correlation following the simple functional form:

$$\left( Nu_{av}, \dot{m}_{in} \right) = a \kappa^b Ra^c \quad (16)$$

Is proposed, where the parameters  $a$ ,  $b$  and  $c$  are  $N$ -dependent. Table 8 shows the parameters for each  $N$ , as they were calibrated with the least-squares method [41]. As expected, the  $Ra$  exponent has the most significant value.

Fig. 11 presents an error analysis between the correlation of eq. (16) and the numerical results. It can be noticed the correlation is very satisfactory for engineering purposes, and its fitness improves for cases with high  $Ra$ . For the range analyzed in the present work, the correlation's determination coefficient is  $R^2 = 0.995$ .

#### 4. Summary and conclusions

This study considered the natural convection inside a square, side-open cavity heated from the side and filled with a fluid and a fixed amount of solid material. The solid material is distributed uniformly inside the cavity via square blocks of progressively increasing number and smaller size (for a constant amount of solid material), arranged in a

**Table 9**  
Average Nusselt number and mass flow rate for various  $Ra$ ,  $N$  and  $\kappa$ .

$Ra$	$10^5$					$10^6$				
	9	16	36	64	144	9	16	36	64	144
$\kappa$	0,1									
$Nu_{av}$	1.668	1.177	0.854	0.699	0.566	10.171	7.713	3.970	2.814	1.999
$\dot{m}_{in}$	4.157	2.974	1.788	1.235	0.683	20.388	15.777	9.168	6.499	4.233
$\kappa$	1									
$Nu_{av}$	1.873	1.523	1.179	1.043	0.939	9.929	7.574	4.551	3.556	2.465
$\dot{m}_{in}$	4.749	3.525	2.104	1.437	0.799	21.257	16.967	10.649	7.997	5.090
$\kappa$	10									
$Nu_{av}$	2.443	2.122	1.802	1.661	1.558	9.665	7.715	5.610	4.434	3.032
$\dot{m}_{in}$	5.700	4.164	2.549	1.710	0.957	22.787	19.003	12.839	9.683	5.961
$\kappa$	100									
$Nu_{av}$	2.667	2.338	1.992	1.856	1.744	9.605	7.906	5.928	4.672	3.205
$\dot{m}_{in}$	5.960	4.325	2.604	1.785	0.999	23.300	19.771	13.459	10.062	6.174
$Ra$	$10^7$					$10^8$				
$N$	9	16	36	64	144	9	16	36	64	144
$\kappa$	0.1									
$Nu_{av}$	26.120	24.668	20.309	13.920	7.554	50.932	50.202	48.975	46.231	34.322
$\dot{m}_{in}$	59.021	53.344	38.196	27.649	17.280	131.033	130.596	116.100	94.183	68.549
$\kappa$	1									
$Nu_{av}$	26.030	24.559	20.136	14.285	9.325	50.700	50.141	48.917	46.143	34.743
$\dot{m}_{in}$	60.690	55.438	41.265	30.959	21.314	146.689	134.377	120.066	99.868	73.931
$\kappa$	10									
$Nu_{av}$	25.783	24.272	20.129	15.793	12.110	50.699	50.000	48.763	45.987	36.299
$\dot{m}_{in}$	64.712	59.107	46.623	36.780	26.760	146.688	141.846	127.556	109.185	86.845
$\kappa$	100									
$Nu_{av}$	25.646	24.137	20.247	16.468	12.891	50.619	49.929	48.683	45.950	37.254
$\dot{m}_{in}$	66.757	60.492	48.545	38.761	28.262	152.771	145.546	130.533	112.857	91.814

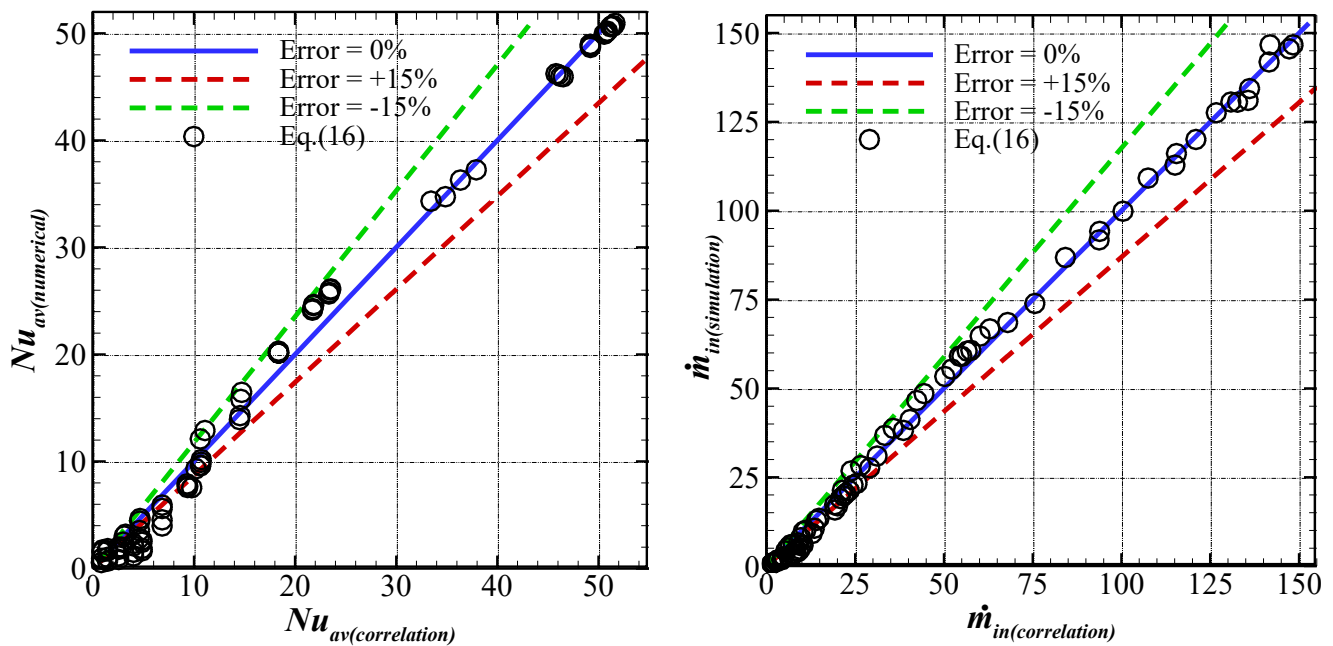


Fig. 11. Fitness of the proposed correlations for a) average Nusselt number and b) mass flow rate entering the cavity.

square lattice. Numerical results are obtained covering a Rayleigh number ( $Ra$ ) range from  $10^5$  to  $10^8$  and a solid-to-fluid thermal conductivity ratio ( $\kappa$ ), from 0.1 to 100. The fluid Prandtl number is set to unity, and the solid-volume fraction inside the cavity fixed as 0.36. Following are the conclusions from the present work:

- With the increase of  $Ra$  from  $10^5$  to  $10^6$ , there is an approximately fourfold increase in  $Nu_{av}$  and an approximately fivefold increase in  $\dot{m}_{in}$ . However, when  $Ra$  is increased from  $10^6$  to  $10^7$ , both  $Nu_{av}$  and  $\dot{m}_{in}$  increase by a factor of four.

- The results indicate an increase in the number of blocks  $N$  (and a corresponding reduction in their size) hinders the natural convection flow entering the cavity. The fluid flows preferentially through the channels available in between the blocks and away from the solid surfaces of the cavity (where flow resistance is higher) – this is the “channeling effect” by the solid blocks.
- The solid refining process (more and smaller blocks) causes the blocks to fall closer to the heated wall, eventually causing an interference (hindrance) on the boundary layer otherwise growing along the hot wall, and a reduction in the heat transfer process.

- This block interference effect is predicted theoretically in terms of the minimum number of blocks beyond which interference should happen for a certain  $Ra$ . The prediction is validated by the observed Nusselt number behavior, justifying why the  $Nu$  variation with  $Ra$  for a fixed  $N$  is not continuous.
- Finally, the last and more complex effect of the blocks, is the fin-like effect. Even forming a discontinuous solid path, the blocks affect the overall diffusion from the hot wall. In this respect, as the thermal conductivity of the solid blocks increases in respect to the fluid thermal conductivity, the diffusion penetrates more toward the hot wall into the cavity opening, enhancing the entire convection process inside the cavity.
- The numerical results in terms of Nusselt number and inlet mass flow rate are tabulated and curve-fit for easy reference and design and analysis utilization.

### Declaration of Competing Interest

The authors declare that they have no known competing financial interests or personal relationships that could have appeared to influence the work reported in this paper.

### Data availability

Data will be made available on request.

### Acknowledgements

The authors from UTFPR gratefully acknowledge the financial support of the Brazilian Coordination for the Improvement of Higher Education Personnel (CAPES) through finance code 001.

### Appendix A

In Table 9, the numerical results for  $Nu_{av}$  and  $\dot{m}_{in}$  are provided for all cases investigated in the present paper to facilitate future comparison work.

### References

- [1] M. Ghalambaz, A. Doostani, E. Izadpanahi, A.J. Chamkha, Conjugate natural convection flow of Ag–MgO/water hybrid nanofluid in a square cavity, *J. Therm. Anal. Calorim.* 139 (3) (2020) 2321–2336.
- [2] R. Fares, F. Mebarek-Oudina, A. Aissa, S.M. Bilal, H.F. Öztop, Optimal entropy generation in Darcy–Forchheimer magnetized flow in a square enclosure filled with silver based water nanofluid, *J. Therm. Anal. Calorim.* 147 (2022) 1571–1581, <https://doi.org/10.1007/s10973-020-10518-z>.
- [3] F. Selimefendigil, H.F. Öztop, Analysis of hybrid nanofluid and surface corrugation in the laminar convective flow through an encapsulated PCM filled vertical cylinder and POD-based modeling, *Int. J. Heat Mass Transf.* 178 (2021) 121623.
- [4] L. Kolsi, F. Selimefendigil, H.F. Öztop, W. Hassen, W. Aich, Impacts of double rotating cylinders on the forced convection of hybrid nanofluid in a bifurcating channel with partly porous layers, *Case Stud. Therm. Eng.* 26 (2021) 101020.
- [5] U.K. Sarkar, N. Biswas, H.F. Öztop, Multiplicity of solution for natural convective heat transfer and entropy generation in a semi-elliptical enclosure, *Phys. Fluids.* 33 (1) (2021) 013606.
- [6] S. Pandey, Y.G. Park, M.Y. Ha, An exhaustive review of studies on natural convection in enclosures with and without internal bodies of various shapes, *Int. J. Heat Mass Transf.* 138 (2019) 762–795, <https://doi.org/10.1016/j.ijheatmasstransfer.2019.04.097>.
- [7] F. Penot, Numerical calculation of two-dimensional natural convection in isothermal open cavities, *Numer. Heat Transf.* 5 (4) (1982) 421–437.
- [8] Y.L. Chan, C.L. Tien, A numerical study of two-dimensional natural convection in square open cavities, *Numer. Heat Transf.* 8 (1) (1985) 65–80.
- [9] Y.L. Chan, C.L. Tien, A numerical study of two-dimensional laminar natural convection in shallow open cavities, *Int. J. Heat Mass Transf.* 28 (3) (1985) 603–612.
- [10] D. Angirasa, J.G.M. Eggels, F.T.M. Nieuwstadt, Numerical simulation of transient natural convection from an isothermal cavity open on a side, *Numer. Heat Transf. Part A Appl.* 28 (6) (1995) 755–767.
- [11] E. Bilgen, A. Muftuoglu, Natural convection in an open square cavity with slots, *Int. Commun. Heat Mass Transf.* 35 (8) (2008) 896–900.
- [12] Z. Wang, M. Yang, L. Li, Y. Zhang, Combined heat transfer by natural convection - Conduction and surface radiation in an open cavity under constant heat flux heating, *Numer. Heat Transf. Part A Appl.* 60 (2011) 289–304, <https://doi.org/10.1080/10407782.2011.594415>.
- [13] M. Montiel Gonzalez, J. Hinojosa Palafox, C.A. Estrada, Numerical study of heat transfer by natural convection and surface thermal radiation in an open cavity receiver, *Sol. Energy.* 86 (2012) 1118–1128, <https://doi.org/10.1016/j.solener.2012.01.005>.
- [14] M. Ouahas, A. Amahmid, M. Hasnaoui, A.E. Mansouri, Y. Dahani, Multi Relaxation Time Lattice Boltzmann Method Simulation of Natural Convection Combined with Surface Radiation in a Square Open Cavity from Three Discrete Heat Sources, *Heat Transf. Eng.* 42 (8) (2021) 706–722.
- [15] G.E. Ovando-Chacon, S.L. Ovando-Chacon, J.C. Prince-Avelino, M.A. Romo-Medina, Numerical study of the heater length effect on the heating of a solid circular obstruction centered in an open cavity, *Eur. J. Mech. B/Fluids.* 42 (2013) 176–185, <https://doi.org/10.1016/j.euromechflu.2013.04.006>.
- [16] A. Lugarini, A.T. Franco, S.L.M. Junqueira, J.L. Lage, Natural convection and surface radiation in a heated wall, c-shaped fracture, *J. Heat Transfer.* 140 (2018), <https://doi.org/10.1115/1.4039643>.
- [17] J.M. House, C. Beckermann, T.F. Smith, Effect of a centered conducting body on natural convection heat transfer in an enclosure, *Numer. Heat Transf. Part A Appl.* 18 (2) (1990) 213–225.
- [18] F.-Y. Zhao, D.i. Liu, G.-F. Tang, Application issues of the streamline, heatline and massline for conjugate heat and mass transfer, *Int. J. Heat Mass Transf.* 50 (1-2) (2007) 320–334.
- [19] P. Bhawe, A. Narasimhan, D.A.S. Rees, Natural convection heat transfer enhancement using adiabatic block: Optimal block size and Prandtl number effect, *Int. J. Heat Mass Transf.* 49 (21-22) (2006) 3807–3818.
- [20] A. Kumar De, A. Dalal, A numerical study of natural convection around a square, horizontal, heated cylinder placed in an enclosure, *Int. J. Heat Mass Transf.* 49 (23-24) (2006) 4608–4623.
- [21] J.Y. Oh, M.Y. Ha, K.C. Kim, Numerical study of heat transfer and flow of natural convection in an enclosure with a heat-generating conducting body, *Numer. Heat Transf. Part A Appl.* 31 (3) (1997) 289–303.
- [22] J.R. Lee, M.Y. Ha, A numerical study of natural convection in a horizontal enclosure with a conducting body, *Int. J. Heat Mass Transf.* 48 (16) (2005) 3308–3318.
- [23] J.R. Lee, M.Y. Ha, Numerical simulation of natural convection in a horizontal enclosure with a heat-generating conducting body, *Int. J. Heat Mass Transf.* 49 (15-16) (2006) 2684–2702.
- [24] F.-Y. Zhao, G.-F. Tang, D.i. Liu, Conjugate natural convection in enclosures with external and internal heat sources, *Int. J. Eng. Sci.* 44 (3-4) (2006) 148–165.
- [25] S.L.M. Junqueira, F.C. De Lai, A.T. Franco, J.L. Lage, Numerical Investigation of Natural Convection in Heterogeneous Rectangular Enclosures, *Heat Transf. Eng.* 34 (2013) 460–469, <https://doi.org/10.1080/01457632.2012.722437>.
- [26] J.L. Lage, S.L.M. Junqueira, F.C. De Lai, A.T. Franco, Aspect ratio effect on the prediction of boundary layer interference in steady natural convection inside heterogeneous enclosures, *Int. J. Heat Mass Transf.* 92 (2016) 940–947.
- [27] A.A. Merrikh, A.A. Mohamad, Blockage effects in natural convection in differentially heated enclosures, *J. Enhanc. Heat Transf.* 8 (2001). <https://doi.org/10.1615/JEnhHeatTransf.v8.i1.50>.
- [28] J.L.L. A.A. Merrikh, Effect of distributing a fixed amount of solid constituent inside a porous medium enclosure on the heat transfer process, in: ICAPM 2004–Proceedings Int. Conf. Appl. Porous Media, 2004: pp. 51–57.
- [29] G. Nascimento, A. Lugarini, E.M. Germer, A.T. Franco, A simple homogeneous numerical solution for nanofluid natural convection in an enclosure with disconnected and conducting solid blocks, *J. Brazilian Soc. Mech. Sci. Eng.* 41 (2019). <https://doi.org/10.1007/s40430-019-1764-1>.
- [30] P.R.M. Santos, A. Lugarini, S.L.M. Junqueira, A.T. Franco, Natural convection of a viscoplastic fluid in an enclosure filled with solid obstacles, *Int. J. Therm. Sci.* 166 (2021), 106991, <https://doi.org/10.1016/j.ijthermalsci.2021.106991>.
- [31] A.A. Merrikh, J.L. Lage, Natural convection in an enclosure with disconnected and conducting solid blocks, *Int. J. Heat Mass Transf.* 48 (7) (2005) 1361–1372.
- [32] I. Battiatto, P.T. Ferrero V, D. O’ Malley, C.T. Miller, P.S. Takhar, F.J. Valdés-Parada, B.D. Wood, Theory and Applications of Macroscale Models in Porous Media, *Transp. Porous Media.* 130 (1) (2019) 5–76.
- [33] D.A. Nield, A. Bejan (Eds.), *Convection in Porous Media*, Springer International Publishing, Cham, 2017.
- [34] S. Whitaker, *The Method of Volume Averaging. Theory and Applications of Transport in Porous Media*, Dordr, Kluwer Acad. Publ. Cited Page. 60 (1999).
- [35] R.B. Bird, R. C., Armstrong, O. Hassager, Dynamics of polymeric liquids, Fluid mechanics, 1987. <https://doi.org/10.1002/pol.1987.140251211>.
- [36] A. Bejan, *Convection Heat Transfer: Fourth Edition*, 2013. <https://doi.org/10.1002/9781118671627>.
- [37] S. V Patankar, *Numerical heat transfer and fluid flow*, 1980.
- [38] H.K. Versteeg, W. Malalasekera, G. Orsi, J.H. Ferziger, A.W. Date, J.D. Anderson, *An Introduction to Computational Fluid Dynamics - The Finite Volume Method*, 1995.
- [39] A. Narasimhan, B.V.K. Reddy, Natural convection inside a bidisperse porous medium enclosure, *J. Heat Transfer.* 132 (2010), <https://doi.org/10.1115/1.3192134>.
- [40] J.F. Hinojosa, R.E. Cabanillas, G. Alvarez, C.E. Estrada, Nusselt number for the natural convection and surface thermal radiation in a square tilted open cavity, *Int. Commun. Heat Mass Transf.* 32 (9) (2005) 1184–1192.
- [41] G. Golub, Numerical methods for solving linear least squares problems, *Numer. Math.* 7 (3) (1965) 206–216.